scientific reports

OPEN

4-methylumbelliferone-mediated polarization of M1 macrophages correlate with decreased hepatocellular carcinoma aggressiveness in mice

Marcelo M. Rodríguez[1], Agostina Onorato[1], María José Cantero[1], Luciana Domínguez[1], Juan Bayo[1], Esteban Fiore[1], Mariana García[1], Catalina Atorrasagasti[1], Ali Canbay[2], Mariana Malvicini[1,4] & Guillermo D. Mazzolini[1,3,4✉]

Hepatocellular carcinoma (HCC) arises in the setting of advanced liver fibrosis, a dynamic and complex inflammatory disease. The tumor microenvironment (TME) is a mixture of cellular components including cancer cells, cancer stem cells (CSCs), tumor-associated macrophages (TAM), and dendritic cells (DCs), which might drive to tumor progression and resistance to therapies. In this work, we study the effects of 4-methylumbelliferone (4Mu) on TME and how this change could be exploited to promote a potent immune response against HCC. First, we observed that 4Mu therapy induced a switch of hepatic macrophages (Mϕ) towards an M1 type profile, and HCC cells (Hepa129 cells) exposed to conditioned medium (CM) derived from Mϕ treated with 4Mu showed reduced expression of several CSCs markers and aggressiveness. HCC cells incubated with CM derived from Mϕ treated with 4Mu grew in immunosuppressed mice while presented delayed tumor progression in immunocompetent mice. HCC cells treated with 4Mu were more susceptible to phagocytosis by DCs, and when DCs were pulsed with HCC cells previously treated with 4Mu displayed a potent antitumoral effect in therapeutic vaccination protocols. In conclusion, 4Mu has the ability to modulate TME into a less hostile milieu and to potentiate immunotherapeutic strategies against HCC.

Hepatocellular carcinoma (HCC) is the 4th cause of cancer-related death worldwide, and its incidence and mortality are increasing steadily[1]. HCC is also the most common cause of death in patients with cirrhosis[2]. Curative therapies are available for a minority of patients with HCC (~ 40%), and although new systemic drugs have been approved for advanced disease (sorafenib and lenvatinib in first line, and regorafenib, cabozantinib and ramucirumab in second-line post sorafenib) their impact on patient survival remain modest[3–5]. Several reports demonstrated that HCC is considered an immunogenic tumor[6,7], and therefore susceptible for immunotherapy-based strategies such as adoptive T cell therapy using tumor infiltrating lymphocytes or peripheral blood mononuclear cells, therapeutic vaccination with dendritic cells (DCs), systemic cytokines, and more recently immune checkpoint inhibitors (ICIs)[8]. The CTLA-4 and PD-1/PD-L1 ICIs have demonstrated efficacy in patients with HCC[9,10]. Based on a potent overall response rate and duration of response, the combination of nivolumab and ipilimumab was recently approved for HCC patients previously treated with sorafenib[11]. However, the suppressive HCC microenvironment is still a major obstacle for an effective antitumor response particularly for immunotherapeutic strategies[12,13]. The tumor microenvironment (TME) is composed by a complex network of tumor cells and stroma components all mixed in an altered extracellular matrix (ECM). TME components include immune cells, cancer-associated fibroblasts (CAFs), tumor-associated macrophages (TAMs) and cancer stem cells (CSCs),

[1]Gene Therapy Laboratory, Facultad de Ciencias Biomédicas, Instituto de Investigaciones en Medicina Traslacional, CONICET-Universidad Austral, Av. Presidente Perón 1500 (B1629ODT) Derqui-Pilar, Buenos Aires, Argentina. [2]Department of Medicine, Universitätsklinikum Knappschaftskrankenhaus Bochum, Ruhr-Universität Bochum, Bochum, Germany. [3]Liver Unit, Hospital Universitario Austral, Universidad Austral, Buenos Aires, Argentina. [4]These authors jointly supervised this work: Mariana Malvicini and Guillermo D. Mazzolini. ✉email: gmazzoli@austral.edu.ar
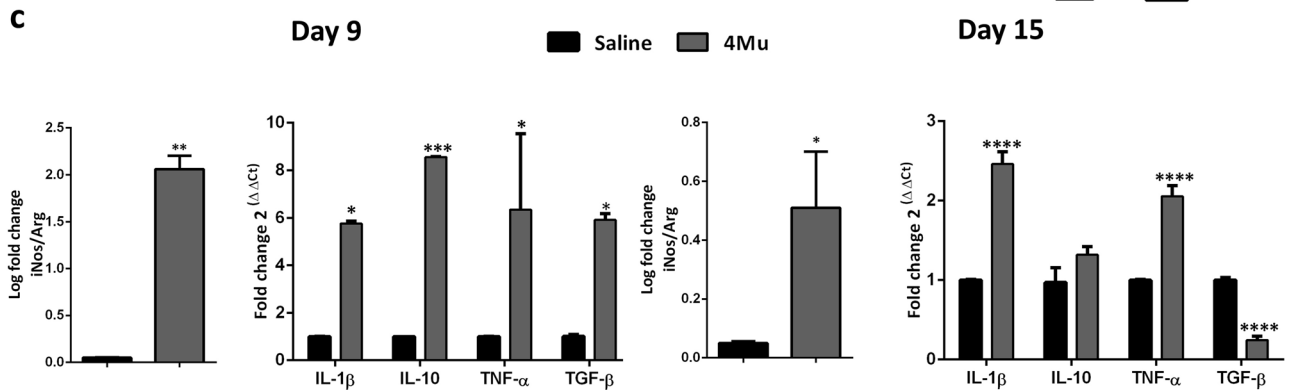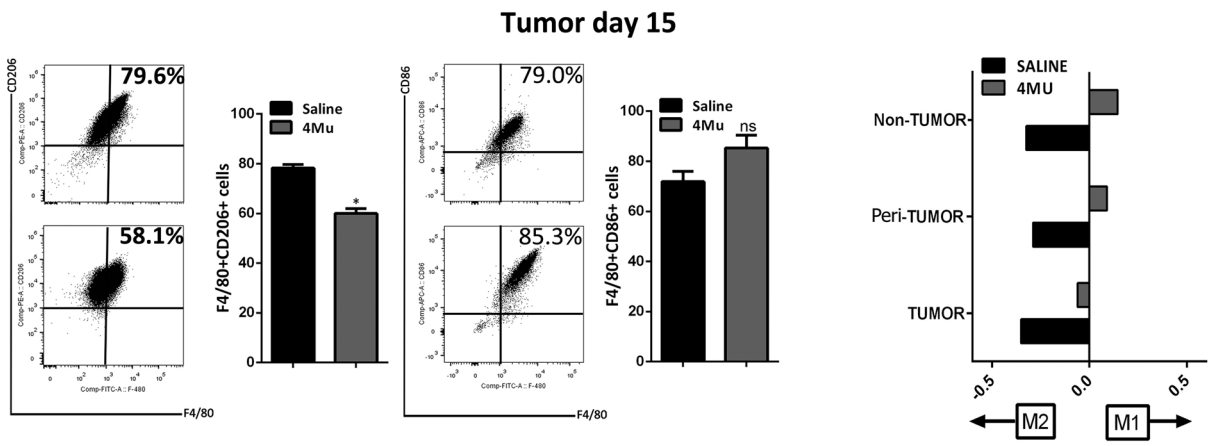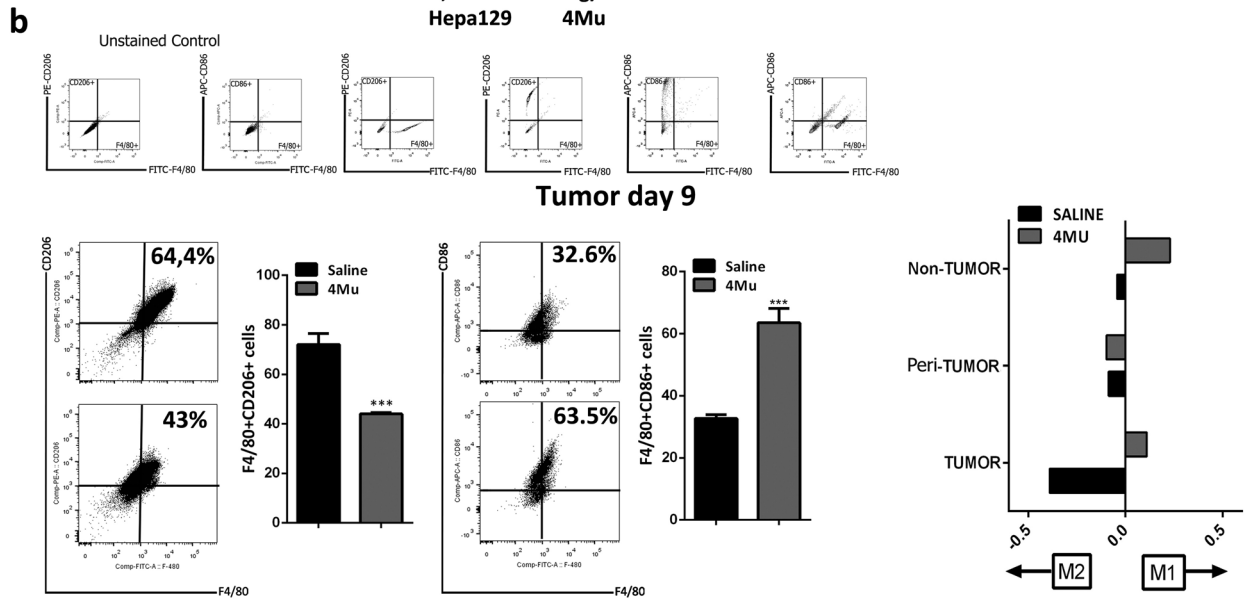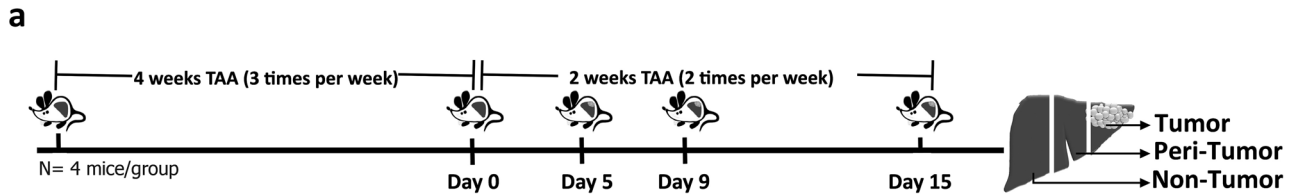
◄**Figure 1.** In vivo modulation of hepatic macrophages expression profile by 4Mu. (**a**) *Left* in vivo experimental model (6 to 8-week-old male C3Hj/He mice; n = 8/group were injected with TAA (200 mg/kg; i.p.) for 4 weeks, 3 times per week, to induce fibrosis. Then, all mice received an intrahepatic inoculation of 1.25×10^5 syngeneic Hepa129 cells (day 0). After tumor implantation, mice received 200 mg/kg 4Mu in drinking water (day 5). On day 9 (n = 4/group) and day 15 (n = 4/group) after 4Mu initiation, mice were sacrificed and liver samples (n = 4/ group) were collected. *Right* The livers were perfused with collagenase and separated in 3 sections (peri-tumoral, tumoral, and non-tumoral tissue). Isolation of non-parenchymal cells from each tissue section was carried out. (**b**) Representative dot plots of flow cytometry analysis using BD Accuri C6 propietary software version 1.0.264.21 (www.AccuriCytometers.com) of auto fluorescence (upper left panels), F4/80+, CD206+ and CD86+ on non-parenchymal cells. Bar graphs showed the percentage of CD206+ F4/80+ (M2), and CD86+ F4/80+ (M1) cells in tumor tissue on day 9 (***p < 0.001) and day 15 (*p < 0.05); 4Mu vs. saline, Mann–Whitney test. Mϕ type1/type2 proportion was calculated as log10 (CD86+/CD206+). (**c**) mRNA expression levels of iNOS, Arg1, IL-1β, IL-10, TNF-α, and TGF-β on isolated Mϕ from tumor tissue samples. iNOS /Arg1 ratio **p < 0.01 and *p < 0.05 4Mu vs. Saline (day 9 and day 15 respectively); Mann–Whitney test; TGF-β, IL-1β and TNF-α *p < 0.05; IL-10 ***p < 0.005; 4Mu vs. saline (day 9); TGF-β, IL-1β and TNF-α ****p < 0.001; 4Mu vs. saline (day 15); two-way ANOVA. Data are expressed as the mean ± SEM. The experiment was carried-out 2 times.

among others[14]. Cellular and non-cellular components of the TME constitute a permissive niche for HCC growth and dissemination[12,14]. It has been reported that type 2 polarized (M2) TAMs suppress antitumor immunity, and the level of infiltrating TAM has been correlated with a poor prognosis[15]. In addition, M2 TAMs release epidermal growth factor (EGF) and transforming growth factor beta (TGF-β), chemokines, metalloproteinases and other cytokines[16]. M2 TAMs are also involved in ECM remodeling, angiogenesis, epithelial-mesenchymal transition (EMT), invasion and metastasis[17]. Furthermore, M2 TAMs interact with other immune cells such as effector lymphocytes promoting resistance against targeted and immunotherapy-based therapies[18,19].

Tumor-initiating or CSCs are a small population of TME cells intimately related to resistance to therapies[20]. CSCs are characterized by the presence of specific markers including CD133, CD44, CD90, EpCAM, CD13, CD47, SOX-2, Wnt, Oct4, among others[21], which are involved in their capacity to initiate tumor growth, to form colonies, and to evade the antitumor immune response[22]. In particular, CD133 is a highly recognized marker for CSCs in HCC, and it has been demonstrated that CD133+ HCC cells have a potent in vivo tumorigenic capacity[23]. It has been observed that TAMs promote HCC development, and support the expansion of CSCs by IL-6 secretion, highlighting the complex interaction between the components of the TME to sustain tumor growth[24].

We have previously reported that the coumarin 4-methylumbelliferone (4Mu) selectively inhibits the synthesis of hyaluronan, a principal component of ECM, exerting antitumor effect against HCC in mice[25]. In this work, we wanted to study the effects of 4Mu on the phenotype and composition of hepatic TAMs, and to analyze the cross-talk between hepatic TAMs and CSCs, and to assess how this molecule is able to modulate the TME milieu to increase the action of the immune system.

Results

In vivo 4Mu therapy induces hepatic macrophages polarization towards a M1 profile.
Macrophages (Mϕ) are major components of TME, and they have a pivotal role in promoting HCC progression[26]. We have studied the effects of 4Mu on hepatic Mϕ population in our experimental model of HCC with associated-fibrosis[25]. After 4 weeks of TAA administration, mice were inoculated orthotopically with 1.25×10^5 Hepa 129 cells (day 0). On day 5, animals received daily saline or 4Mu orally (200 mg/kg; Fig. 1a, *Left*). On day 9 and 15 mice were sacrificed, and liver sample collected. The fraction of non-parenchymal cells from tumor, peri-tumor, and non-tumor liver regions (Fig. 1a, *Right*) were obtained and analyzed by flow cytometry. The percentage of F4/80+CD206+ and F4/80+CD86+ cells was evaluated and the M1/M2 proportion was calculated as log10 (CD86+/CD206+). 4Mu therapy induced a polarized M1 profile in tumor and non-tumor sections in comparison with saline group (Fig. 1b, *Right*) on day 9. In addition, we observed a M1 Mϕ profile induced by 4Mu in peri-tumor and non-tumor sections on day 15; Fig. 1b also showed the reduced percentage of F4/80+CD206+ cells (44.0 ± 0.63% vs. 72.0 ± 4.41%; ***p < 0.001 and 60.0 ± 1.90% vs. 78.2 ± 1.43%, *p < 0.05 4Mu vs. saline, respectively. This effect is accompanied by an increase in the percentage of F4/80CD86+ cells in tumor pieces (63.5 ± 4.63% vs. 32.6 ± 1.24%; *p < 0.05 and 85.2 ± 5.22% vs. 71.8 ± 4.12%; *p < 0.05 4Mu vs. saline) induced by 4Mu on day 9 and day 15, respectively. We also found that the ratio of mRNA levels of iNOS/Arg1 in hepatic Mϕ isolated from tumor sections of 4Mu treated mice was enhanced both at day 9 and at day 15 (**p < 0. 01 on day 9; *p < 0.05 on day 15; Fig. 1c). Although the levels of cytokines modulated in tumor hepatic Mϕ on day 9 did not show clearly a definitive profile, there was a significant increase in the mRNA levels of IL1-B and TNF-α together with a decrease of TGF-β and IL-10 on day 15, which means a clear polarization induced in tumor hepatic M towards an M1 profile after 4Mu treatment (Fig. 1c).

4Mu modifies the macrophages profile towards a pro-inflammatory phenotype.
Under conditions of an immunosuppressive TME, stroma cell-derived factor 1 (SDF-1), secreted by activated hepatic stellate cells (HSCs) and tumor-derived vascular endothelium growth factor (VEGF) regulate TAMs recruitment and induce their polarization toward an M2 profile[14]. We have previously reported that 4Mu decreased the activation of HSCs leading to a reduction in the degree of liver fibrosis in mice[27], and a decrease in the production of VEGF, SDF-1 and IL-6[28]. Then, we wonder whether the hepatic Mϕ profile generated upon 4Mu therapy might be due to a direct effect on hepatic Mϕ. To elucidate this, we in vitro cultured isolated peritoneal Mϕ (pMϕ) from healthy micewith 4Mu. After 72 h, we tested F4/80+CD86+ and F4/80+CD206+ cells by flow cytometry, and measured mRNA levels of M1 and M2 cytokines. We observed that 4Mu reduced the percentage of F4/80+CD206+ in

comparison with control (12.1 ± 0.81 vs. 25.0 ± 4.42, *$p < 0.05$, day 9; and 17.6 ± 2.83 vs. 39.3 ± 1.61, *$p < 0.05$, day 15, Mann–Whitney test) (Fig. 2a). We observed that pMɸ treated in vitro with 4Mu showed a fivefold increase in the ratio iNOS/Arg1 (*$p < 0.05$, 4Mu vs. RPMI; Mann–Whitney test). In addition, the mRNA levels of pro-inflammatory cytokines were significantly increased (****$p < 0.001$ and ***$p < 0.005$ respectively; 4Mu vs. RPMI, two-way ANOVA test) while mRNA levels of IL-10, understanding that pMɸ from male mice can express high levels of IL-10[29], were reduced (****$p < 0.001$; Fig. 2b). These results suggest a direct effect elicited by 4Mu on Mɸ profile.

Then, we assessed whether the effect of 4Mu on hepatic Mɸ polarization could be monitored by studying pMɸ. Mice with fibrosis-associated HCC were treated or not with 4Mu, and pMɸ were obtained at days 9 and 15. 4Mu treatment induces an increase in M1/M2 profile both at day 9 and 15 after therapy (Fig. 2c, *Left*). The dot plot graph showed the representative percentage of F4/80+CD206+ and F/480+CD86+ cells on pMɸ obtained from treated HCC-bearing mice (Fig. 2c, *Right*). To validate the antitumor effect induced by 4Mu in our model, mice were sacrificed, and tumor growth was analyzed. Figure 2d showed the efficacy of 200 mg/kg 4Mu on orthotopic HCC tumor nodules. Finally, we assessed the percentage of tumor infiltrating T cells, as they play a key role after M1 polarization induced by 4Mu. Figure 2e illustrated that 4Mu improved the percentage of CD3+CD4+ ($5.64 \pm 0.48\%$ vs. $3.71 \pm 1.43\%$; ns, 4Mu vs. Saline) and CD3+CD8+ T cells ($35.6 \pm 7.01\%$ vs. $6.25 \pm 1.34\%$; (***$p < 0.001$, 4Mu vs. Saline; Mann–Whitney Test) in tumor tissue sections from treated mice in comparison with non-treated mice We also observed that 4Mu therapy was able to induce a significant decrease of splenic Gr1+CD11b+ myeloid derived suppressor cells (MDSCs), and CD4+Foxp3+ Regulatory T cells (Tregs) levels in HCC-bearing mice (Supplementary Fig. S2).

Effect of M1 macrophages polarization induced by 4Mu on hepatocarcinogenesis.

We next aimed to evaluate if the M1 phenotype of Mɸ induced by 4Mu has effects on the capability of HCC cells to establish and growth. To this end, s.c. tumors were developed in C3H/He mice with Hepa129 cells cultured in the presence of CM derived from pMɸ treated or not with 4Mu (4Mu-treated pMɸ derived CM). Remarkably, we found a high index of tumor development and progression in Hepa129 control tumors generated by cells incubated with either RPMI or with CM derived from untreated pMɸ. On the other hand, the growth of tumors established from Hepa129 cells pre-treated with 4Mu-treated pMɸ derived-CM was significantly reduced (Fig. 3a) Then, we wanted to study if tumor aggressiveness was modified by 4Mu-treated pMɸ derived CM and untreated pMɸ-derived CM). We observed that after 24 h and 48 h of pre-conditioning, 4Mu-treated pMɸ derived-CM reduced the expression levels of cancer stemness markers (TLR4 and CD47)[30,31], and the totipotency factor Sox2[32] in cells (*$p < 0.05$, **$p < 0,01$ and ****$p < 0,001$; Kruskal–Wallis test) (Fig. 3b). As we described, HCC are composed of subpopulations of tumor cells with diverse tumorigenic abilities[33]. Then, we magnetically isolated CD133+ and CD133- Hepa129 cells to compare if CM mediate a differential effect mainly on CSCs. Figure 3c showed that 24 h of pre-conditioning with 4Mu treated-pMɸ derived-CM has no effect on the CSCs markers levels while 48 h of pre-conditioning with 4Mu treated-pMɸ derived-CM strongly reduces levels of TLR4, CD47 and Sox2 expression on CSCs. In addition, CM derived from 4Mu-treated pMɸ showed a reduced amount of IL-6 in comparison with untreated pMɸ (Fig. 3d).

We next administrated Hepa 129 cells exposed to CM from 4Mu treated-pMɸ in athymic Nu/Nu mice. The results showed that tumor progression in immunosuppressed mice with Hepa129 cells pretreated with pMɸ derived-CM or 4Mu treated-pMɸ derived-CM were similar to controls (Fig. 4a).

We previously demonstrated that 4Mu does not show a significant impact on Hepa129 cell growth and survival. However, 4Mu can modulate the expression of CSCs markers, particularly CD47, contributing to the phagocytosis of CD133+ CSCs[25]. Based on this, modulation of CD47 expression might have a dual effect, on one side induces a less aggressive tumor phenotype and, on the other side, HCC cells might become more susceptible to the recognition by the immune system. Figure 4b,c reveal that CD133+ cells could generate tumors in both immunocompetent and immunocompromised mice. In contrast, when the expression of CD47 is inhibited by 4Mu, tumors progressed only in immunocompromised animals while were potently controlled in immunocompetent mice.

4Mu stimulates antigen presentation by dendritic cells and improves their capability to phagocyte cancer cells.

We assessed whether 4Mu have effects on the function of dendritic cells (DCs). First, we performed an in vitro phagocytosis assay using BM-derived DCs from C3H/He mice. Hepa129 HCC cells were labeled with DAPI, co-cultured with DCs for 2 h, and incubated with MHC II and CD86 antibodies. We quantified the presence of MHC II+ CD86+ DCs, gated them, and then identified MHCII+CD86+DAPI+ phagocyted Hepa 129 cells (Fig. 5a, *Right*). Interestingly, phagocytosis was significantly increased in Hepa129 + 4Mu cells compared with untreated Hepa129 cells (Fig. 5a, *Left*; 36.4 ± 3.69 vs. 24.8 ± 3.40; *$p < 0.05$, Mann–Whitney test). We also observed that 4Mu could facilitate the maturation of DCs since the percentages of CD11+MHCII+CD86+ DCs were higher when DCs were exposed to 4Mu for 72 h (Supplementary Fig. S3). This result suggests that the ability to recognize tumor cells by DCs is increased by 4Mu.

Therapeutic vaccination using 4Mu treated-tumor-pulsed dendritic cells delayed HCC growth.

We studied the effect of a therapeutic vaccine generated with DCs pulsed with 4Mu treated Hepa129 whole tumor lysates. Then, we injected DCs pulsed with Hepa129 tumor lysates obtained from 4Mu- or vehicle-treated mice (DCs/Hepa129/4Mu or DCs/Hepa129 respectively; i.p.) in C3H/He tumor-bearing mice. Figure 5b showed that vaccination with DCs/Hepa129/4Mu induced a potent antitumoral effect in comparison with DCs/Hepa129 (*$p < 0.05$; Kruskal–Wallis test). Additionally, DCs/Hepa129/4Mu therapy significantly increased the animal survival when compared to control mice (Fig. 5c; Log-rank test *$p < 0.01$). To validate these results,
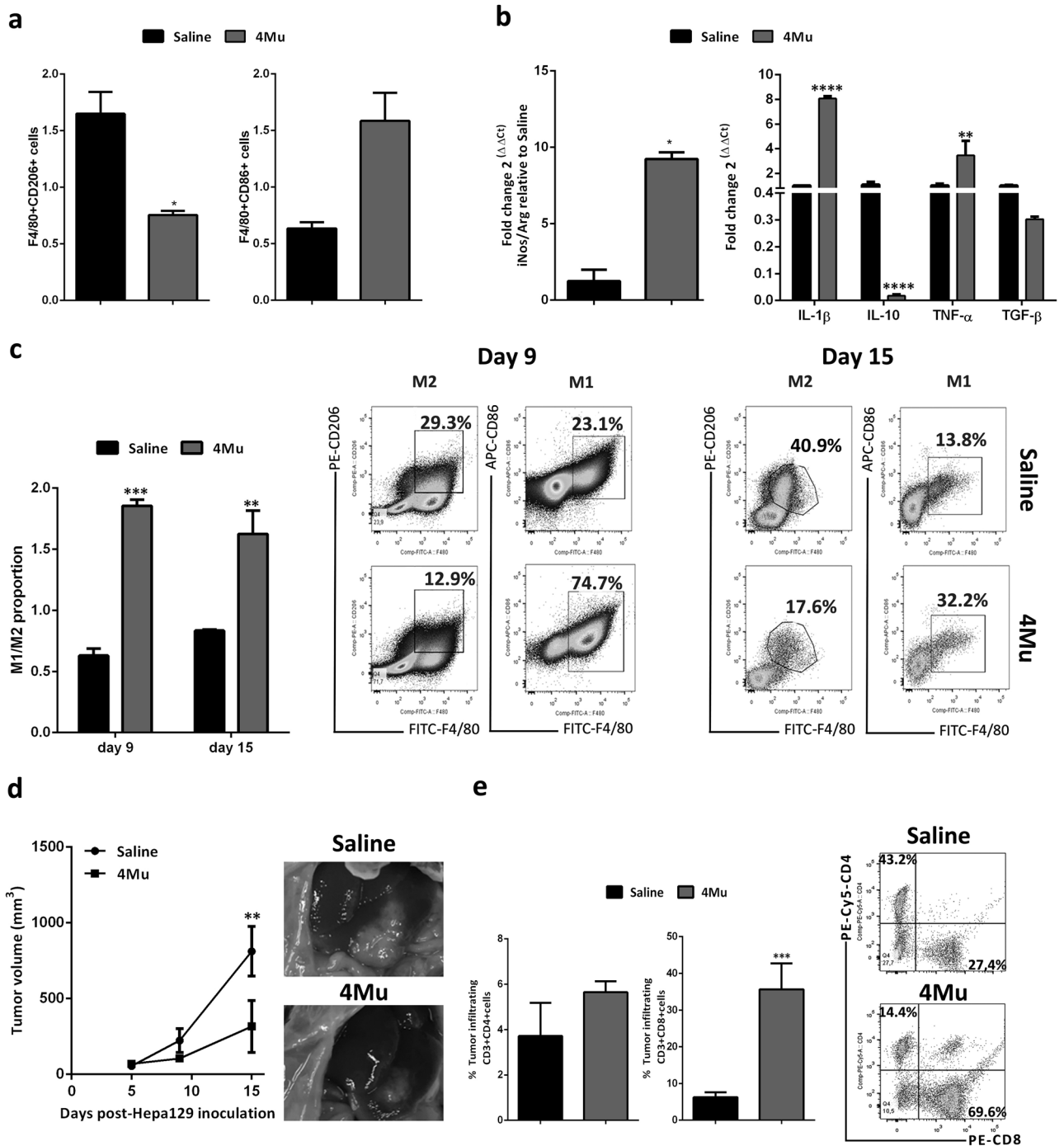
Figure 2. Type 1 macrophages phenotype was induced by 4Mu. (**a**) Peritoneal macrophages (pMφ) were isolated from healthy mice (n = 4), cultured with 0.5 mM 4Mu for 72 h (n = 2), stained with anti-F4/80, anti-CD86 and anti-CD206 antibodies, and analyzed by flow cytometry. (**b**) iNOS/Arg1 ratio, and cytokine gene expression were measured in pMφ by qPCR (*p < 0.05; **p < 0.01; ****p < 0.0001 4Mu vs. saline; Mann–Whitney test and two-way ANOVA test respectively). (**c**) In vivo effects of 4Mu on pMφ in mice (n = 4/group) with fibrosis-associated HCC. pMφ were obtained on day 9 (n = 2) and 15 (n = 2). Flow cytometry of F4/80+ CD86+ and CD206+ cells were analyzed, and the M1/M2 proportions were calculated as log2 (CD86+/CD206+);***p < 0.001, **p < 0.01 4Mu vs. saline, on days 9 and 15, respectively; Mann–Whitney test. (**d**) Tumor volume was measured on 4Mu treated and non-treated tumor-bearing mice at day 9 (p = 0.0571; ns) and at day 15 (**p < 0.01; Unpaired T Test). (**e**) Lymphocytic infiltration of HCC tumors. Flow cytometry analysis of CD4 and CD8 T cells. Percentage of CD8+ cells ***p < 0.001 4Mu vs. saline, Mann–Whitney Test. Data are expressed as the mean ± SEM. Flow cytometry was analyzed using BD Accuri C6 propietary software version 1.0.264.21 (www.AccuriCytometers.com) The experiments were repeated 2 times.
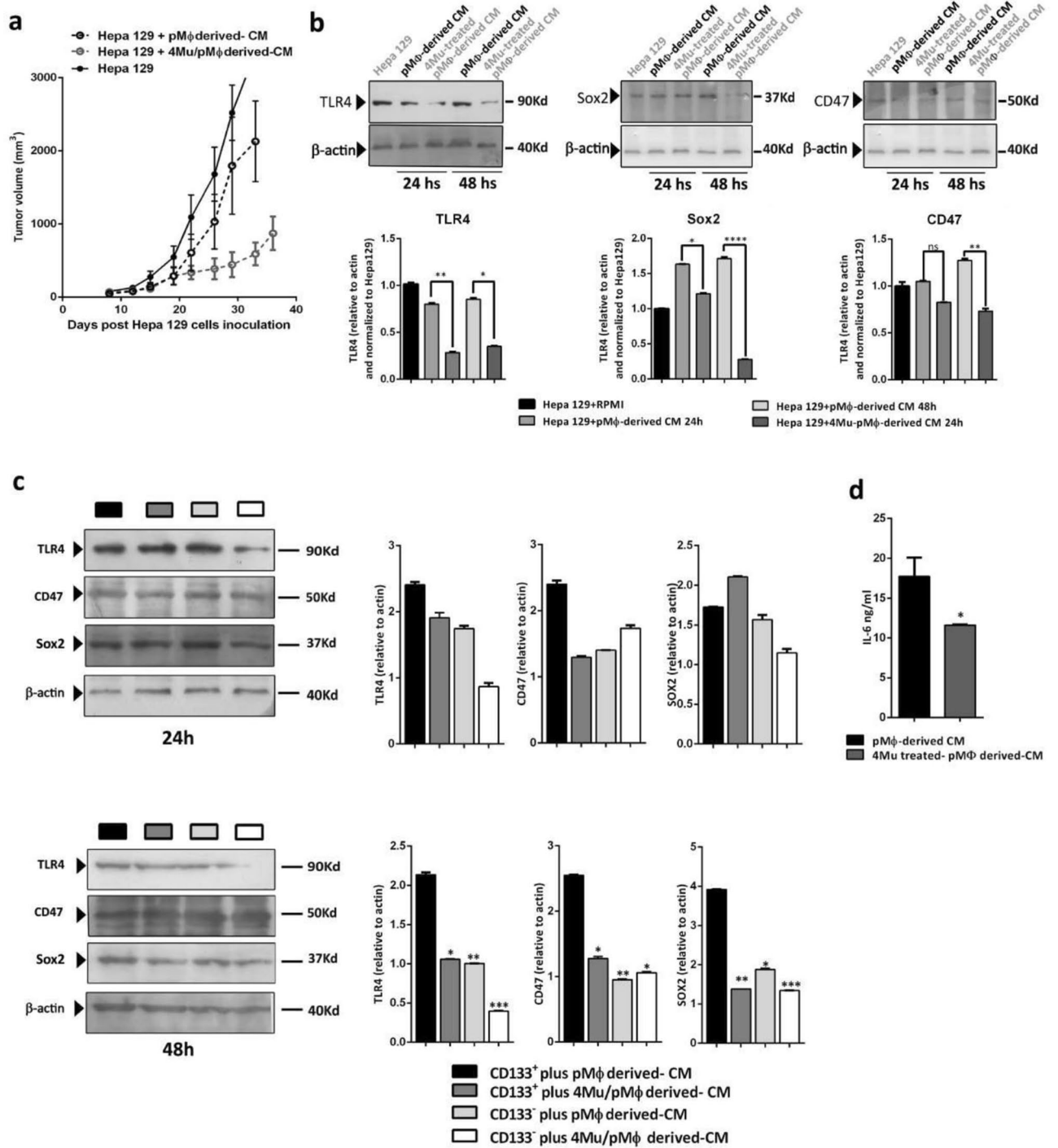
Figure 3. M1 type macrophages induced by 4Mu ameliorate hepatocellular carcinoma aggressiveness. (**a**) Hepa129 cells were incubated for duplicate with RPMI (Hepa129 + RPMI), CM from isolated pMφ (Hepa129 + pMφ-derived CM), and CM from isolated pMφ in vitro treated with 4Mu (Hepa129 + 4Mu-treated pMφ-derived CM) for 48 h. Pre-conditioned 1×10^6 Hepa 129 cells were injected s.c. in C3Hj mice (n = 4/ group), and tumor volume was measured. (**b**) Hepa129 cells were cultured with RPMI, pMφ-derived CM and 4Mu-treated pMφ-derived CM, and the expression levels of TLR4, CD47 and Sox2 were analyze by western blot; different parts from different membranes were delineated with dividing lines. Full-length blots are presented in Supplementary Fig. 4A **p < 0.05, *p < 0.01 or ****p < 0.001; Kruskal-Wallys test. (**c**) TLR4, CD47 and Sox2 expression was also determined by western blot on magnetic-isolated CD133+ and CD133- Hepa129 cells cultured with pMφ-derived CM or 4Mu-treated pMφ-derived-CM; different parts from different membranes were delineated with dividing lines. Full-length blots are presented in Supplementary Fig. S4B, **p < 0.01CD133 + plus 4Mu-treated pMφ-derived-CM vs. pMφ-derived CM; 48hs Kruskal–Wallys test. (**d**) IL-6 production by pMφ treated or not with 4Mu in vitro by ELISA, *p < 0.05 Unpaired T test; Data are expressed as the mean ± SEM. The in vivo and in vitro experiments were carried-out 2 times.
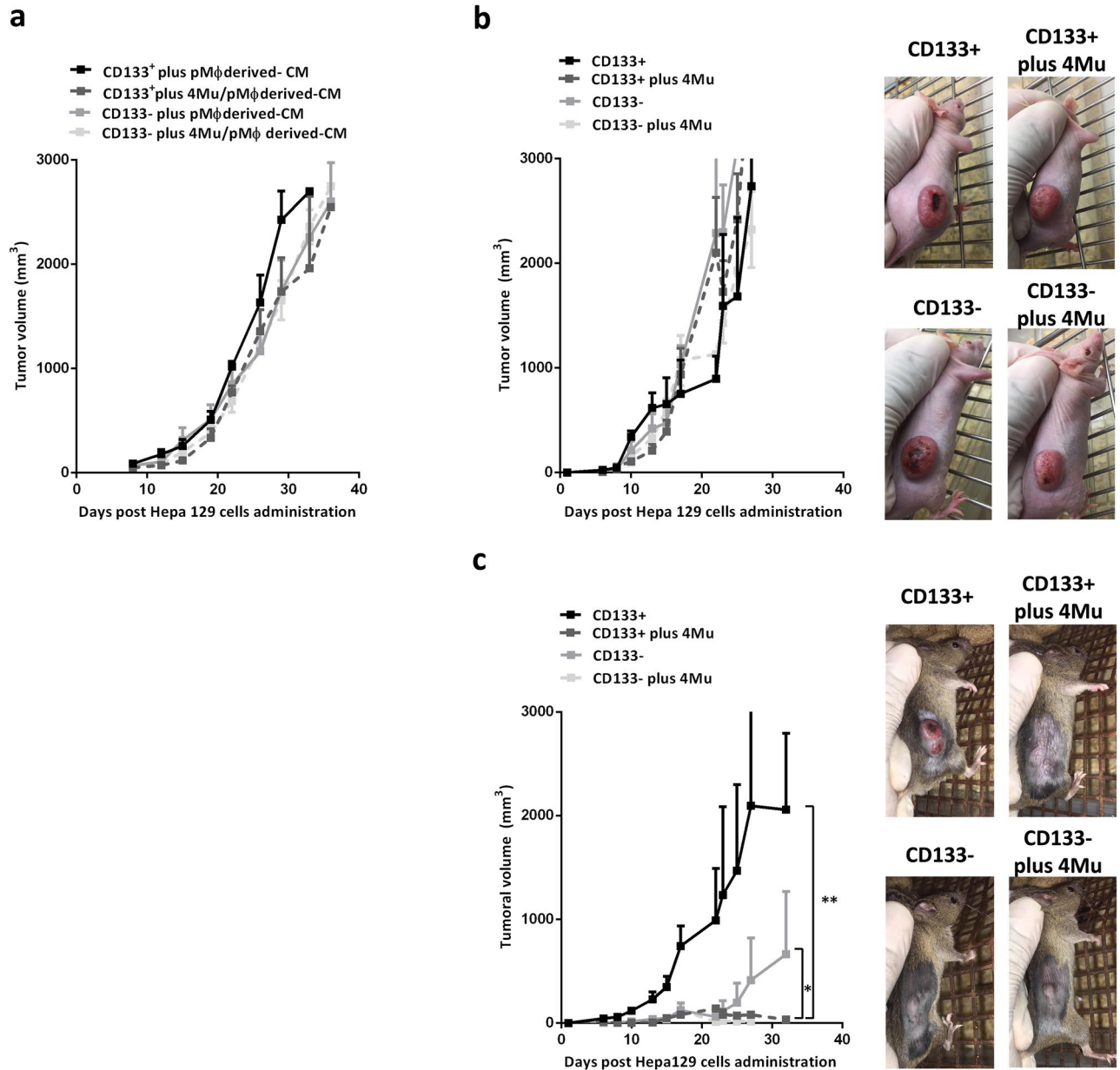
Figure 4. 4Mu and M1 hepatic macrophages facilitate immune recognition of CD133+ HCC cells, and promote antitumor response. (**a**) Hepa129 cells were incubated for duplicate with RPMI (Hepa129 + RPMI), CM from isolated pMφ (Hepa129 + pMφ-derived CM) and CM from isolated pMφ in vitro treated with 4Mu (Hepa129 + 4Mu-treated pMφ-derived CM) for 48 h. Pre-conditioned 1×10^6 Hepa129 cells were injected s.c. in Nu/Nu mice (n = 4/group), and tumor volume was measured. (**b**) Nu/Nu mice (n = 4) and (**c**) immunocompetent C3Hj mice (n = 4) were injected s.c. with 1×10^5 CD133 + Hepa129 cells, 1×10^5 4Mu-treated CD133+ Hepa129 cells, 1×10^5 CD133-Hepa129 cells, and 1×10^5 4Mu-treated CD133- Hepa129 cells. Tumor volume was monitored by caliper. **p < 0.01 CD133+ vs. 4Mu-treated CD133+; *p < 0.05 CD133- vs. 4Mu-treated CD133+; Tukey's multiple comparisons test. Data are expressed as the mean ± SEM. The experiment was carried-out 2 times.

we also evaluated the activity of DCs vaccination in a murine cholangiocarcinoma (BNL cells) model. In this case, mice that received DCs pulsed with tumors treated with 4Mu also showed a significant decrease in tumor growth and an increase in animals survival (Fig. 5d,e; *p < 0.05, Kruskal–Wallis test; *p < 0.01, Log-rank test respectively).
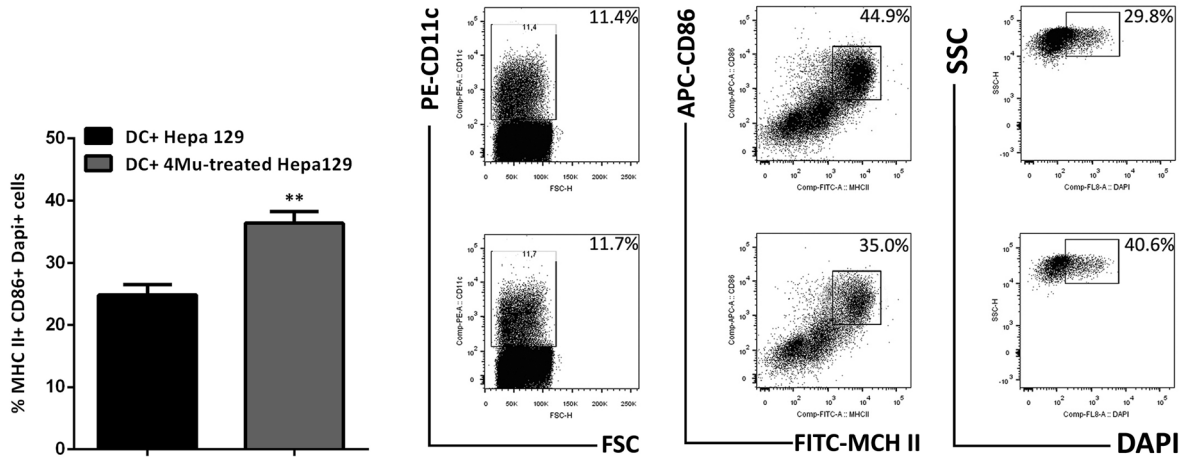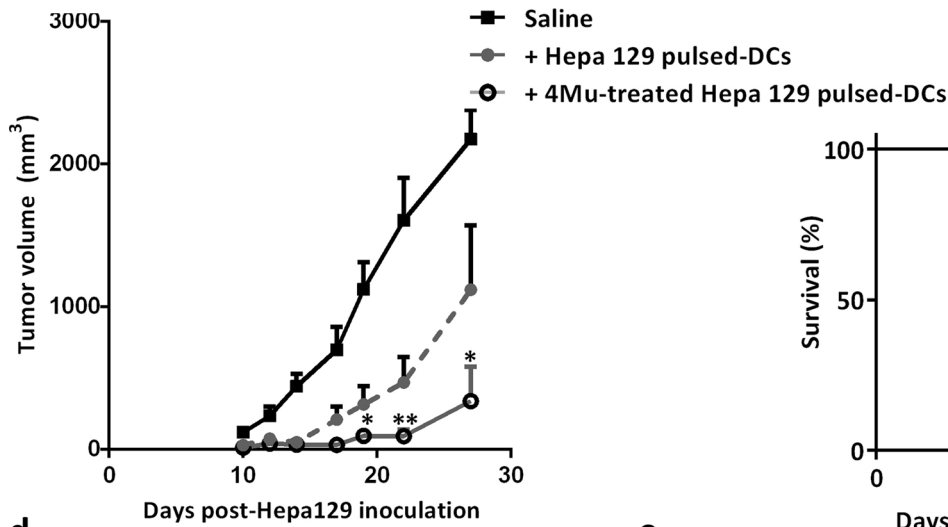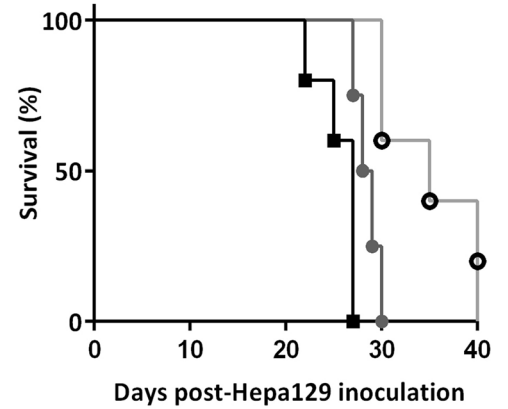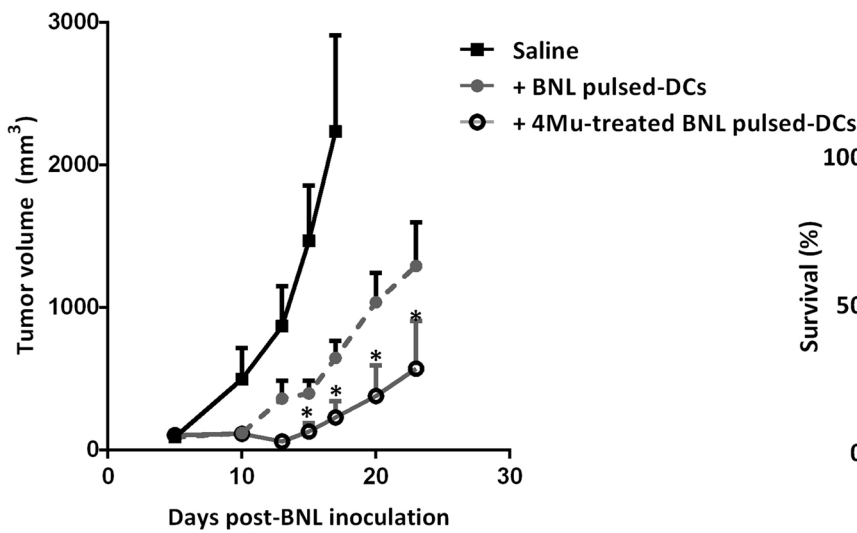
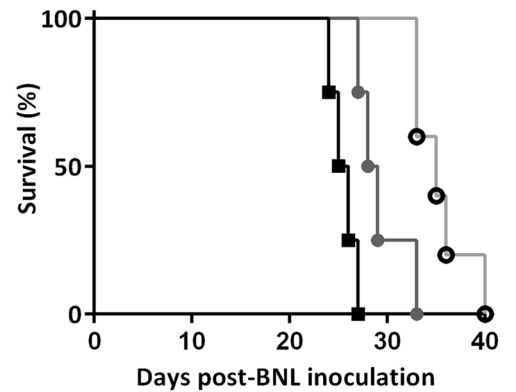◄**Figure 5.** 4Mu preconditioning of HCC cells increases phagocytosis of Hepa129 cells by DCs promotes a potent antitumoral response. (**a**) DCs was derived from bone marrow of C3H/j mice, and incubated for 7 days in presence of GM-CSF and IL-4. Hepa129 cells were treated with 4Mu for 72 h. Phagocytosis assay of DCs was performed by incubation with DAPI + Hepa129 cell (1:4). The analysis of the percentage of MHCII⁺CD86⁺DAPI⁺ (right) was performed using flow cytometry *p < 0.05 4Mu vs. RPMI (left), Mann–Whitney test. Data are expressed as mean percentage ± SD. (**b**) C3Hj mice were s.c. inoculated with 1×10^6 Hepa 129 cells (n = 4–5/group); on day 9, mice were peritumorally injected with 1×10^6 4Mu-treated tumor-pulsed DCs, tumor-pulsed DCs o saline *p < 0.05 4Mu-treated Hepa 129-pulsed DCs vs. Saline; (**c**) Kaplan–Meier survival curve of the mice bearing Hepa 129 tumors. (**d**) BALB/c mice (n = 4/group) were s.c. inoculated with 1×10^6 BNL cells; on day 9, mice were peritumorally injected with 1×10^6 4Mu-treated BNL- pulsed DCs, BNL-pulsed DCs o saline. *p < 0.05 4Mu-treated BNL-pulsed DCs vs. Saline; ANOVA and Tukey's test. (**e**) Kaplan–Meier survival curve of the mice bearing BNL tumors. Tumor volumes were measured 3 times a week over a period of 30 days. The growth curve is representative of 3 independent experiments (mean ± SD).

Discussion

In the last years, the study of the TME components on carcinogenesis has gained an special interest due their potential as therapeutic targets[34]. Different cellular components of the TME could act in synergy to facilitate cancer progression and to avoid the immune system recognition. In particular, TAMs population and their activation status are involved in tumor aggressiveess[15]. The classical Mφ activation M1 type is characterized by the expression of the co-stimulatory molecule CD86, an increase in the activity of iNOS, and in the production of pro-inflammatory cytokines such as IL-1β and TNF-α. On the other hand, the alternative type 2 polarized Mφ (M2) is known by the expression of CD206, an increased activity of arginase I, and by the release of the anti-inflammatory cytokines IL-10 and TGF-β[17].

Hepatic Mφ play an essential role in the pathogenesis of chronic inflammatory liver diseases, and in the progression of HCC[26,35]. TAMs are one of the more abundant immune cells that infiltrate tumors. Yeung et al. described a direct effect M2 Mφ on HCC growth. They showed that the expansion of TAMs with M2 phenotype promote tumor growth and invasiveness through the release of CCL22. Moreover, the peritumoral accumulation of M2 Mφ observed in patient samples correlates with poor prognosis, and constitutes a predictor of patient survival[15].

The role of circulating stem cell-like tumor cells phenotypes in HCC was addressed by Sun et al. They observed that the presence of circulating HCC cells with a stem-like phenotype (Epcam⁺/CD133⁺) was associated with recurrence in HCC patients after surgery[36]. In addition to CCL22, it has been demonstrated that M2 TAMs also secrete TGF-β and IL-6 promoting EMT and acquisition of CSCs-like properties[24,37]. IL-6 detected in human HCC samples correlated with the presence of CSCs markers, and IL-6 expressed by TAMs induces the expansion of CD44⁺ cells in culture[24].

Our previous results showed that 4Mu mitigates thioacetamide-induced liver chronic injury by reducing hyaluronan deposition, and hepatic stellate cells activation. 4Mu therapy also inhibited angiogenesis and tumor growth in vivo[28,38]. In the present work, we demonstrated that 4Mu modified the hepatic Mφ phenotype. and their cytokine secretion profile. While a typical M2 activation was found in Mφ from tumor, peri-tumor, and non-tumor tissues of untreated HCC, there was a significant M1 polarization induction in tumoral Mφ after 4Mu treatment. When HCC cells were cultured in presence of supernatant from 4Mu-induced M1 Mφ, and challenge immunocompetent mice with this preconditioned HCC cells, a delayed tumor progression was observed. This data suggests that 4Mu modulates the ability of hepatic Mφ to promote tumor growth. Remarkably, CM derived from Mφ treated with 4Mu induces a significant reduction of stemness-related markers on both whole HCC cells and more significant on isolated CSCs.

Recently, it has been reported that increased expression of CD47 on HCC cells was positively correlated with the density of hepatic Mφ, and with poor clinical prognosis[39]. In this work, the authors also suggested that IL-6 derived from hepatic TAMs was involved in the up regulation of CD47 expression on HCC cells. In this line, we observed in our model that CM derived from Mφ treated with 4Mu showed lower levels of IL-6, and that 4Mu reduced the stemness-related phenotype on HCC cells and their capacity to growth in vivo after the exposure to CM derived from Mφ treated with 4Mu.

Conditioned media from Mφ treated with 4Mu induced a less aggressive HCC phenotype and facilitated immune system recognition. We also demonstrated that CD133⁺ CSCs generate tumors in both immunocompetent and immunocompromised mice, but when the expression of stemness-related markers is inhibited by 4Mu, tumors grew only in athymic animals while were susceptible to the immune system control in immunocompetent mice.

It has been proposed that hepatic M2 Mφ interact with cytotoxic CD8⁺ T cells, and induce resistance to immunotherapy. In addition, a positive association was demonstrated between the expression levels of M2 Mφ markers, decreased CD8⁺ T cell infiltration, and PD-L1 levels in tumor pieces from patients with HCC[19]. In our hands, M1 polarization was induced in HCC tumors after 4Mu treatment, the percentage of CD3⁺CD8⁺ tumor infiltrating T cells was increased, and by the reduction of CD47 expression on CSCs they might result more "visible" to the immune system, open the possibility to combine 4Mu with other immunotherapies like checkpoints inhibitors[40].

Drug resistance was reported in advanced HCC patients treated with standard tyrosine kinase inhibitors (TKI)[3,41]. Sorafenib-resistant clones derived from HCC cell lines showed CSCs properties, including up-regulation of CD47. In addition, CD47 expression was found to be regulated by nuclear factor kappa B (NF-κB), and human HCC samples showed a positive correlation between NF-κB and the presence of CD47[42]. Modulation of CSCs markers, particularly CD47, directly by 4Mu or indirectly through the induction of M1 hepatic Mφ

generated by 4Mu could be considered as an approach to sensitize cancer cells to TKI therapy, particularly in patients who have been previously treated with sorafenib.

We showed that 4Mu decreases CD47 expression on HCC cells and facilitates phagocytosis by Mϕ, which is also associated with antitumor immune response in mice. It has been reported a role of SIRP-expressing DC in antitumor responses, including in HCC; it is possible that CD47 down regulation by 4Mu may affect the response mediated by both macrophages and DC. Here, we have also described that 4Mu has the ability to turn DCs more active to recognize and engulf tumor cells. It have been reported that DCs migrate into tumor-draining lymph nodes and prime CD8+ or CD4+ T cells to induce antitumor responses in mouse models, although their manipulation in cancer vaccination protocols has not reached a potent clinical impact[43,44]. Tumor progression was significantly inhibited in mice that receive DCs pulsed with 4Mu-treated HCC lysate in comparison with mice DCs pulsed with HCC lysate alone, suggesting that 4Mu therapy increases the potential of DCs to generate immunity against HCC. Dendritic cell-based vaccines have been tested as therapeutic tool for HCC[45]. A recently reported meta-analysis aimed to investigate the efficacy of DCs alone or combined with conventional treatments illustrated that cellular immunotherapy improve prognosis by increasing overall survival and reducing recurrence in patients with advanced HCC[46].

All in all, our results suggest that 4Mu exerts a significant antitumoral effect: (i) by inducing a switch of hepatic Mϕ into a M1 profile, (ii) by reducing their capacity to secrete IL-6, (iii) by increasing HCC recognition by the immune system upon incubation of tumor cells with CM derived from Mϕ treated with 4Mu; (iv) by reducing the expression of several CSCs markers on HCC cells; and (v) by increasing the ability of DCs to inhibit HCC tumor growth in therapeutic vaccination protocols. In conclusion, our data highlight the potential of 4Mu to modulate the TME facilitating the induction of an immune response against HCC.

Materials and methods

Animals.
Six-to-eight-week-old male C3Hj/He, BALB/c and athymic N:NIH(S)-nu mice (Nu/Nu) mice were purchased from Centro Atómico Ezeiza (Buenos Aires, Argentina). Animals were maintained at our Animal Resources Facilities in accordance with the experimental ethical committee and the NIH guidelines on the ethical use of animals. The Animal Care Committee from School of Biomedical Sciences, Universidad Austral, approved the experimental protocol (protocol #2018-05) which was based on the essential points of the ARRIVE guidelines.

Cell lines.
Hepa129 cells (HCC cells syngeneic with C3H/He mice) were kindly provided by Dr. Volker Schmitz (Bonn University, Germany). BNL cells (cholangiocarcinoma cells, syngeneic with BALB/c mice) were provided by Prof. Dr. Jesús Prieto (CIMA, Spain). Hepa129 and BNL cells were grown in RPMI 1640 (GIBCO-Fisher Scientific, UK) with 10% fetal bovine serum (FBS).

Drugs.
4 Methylumbelliferone (4Mu) sodium salt was purchased from Sigma-Aldrich (USA)[28].

In vivo experiments.
Experimental model of HCC associated with fibrosis. C3H/He mice received 200 mg/kg of thioacetamide (TAA) (Sigma-Aldrich, USA) intraperitoneally (i.p.) 3 times a week for 4 weeks to develop liver fibrosis. TAA-treated livers from tumor-bearing mice showed the extensive appearance of portal–portal and central–portal fibrous septae and distortion of liver architecture (Supplementary Fig. S1). On day 28, mice were anesthetized and orthotopic tumors were established by subcapsular inoculation of 1.25×10^5 Hepa129 cells directly into the left liver lobe by laparotomy[25] (day 0). Five days after tumor implantation, mice were distributed in groups (n = 8/group) and received: (i) saline (control), or (ii) 4Mu 200 mg/kg in the drinking water ad libitum. TAA was administered until mice were used in ex vivo studies. On day 9 and 15 mice were sacrificed, tumor volume was measured using a caliper, and liver samples were collected. In some experiments, livers were perfused with collagenase and separated in 3 sections (peri-tumoral, tumoral, and non-tumoral tissue). Isolation of non-parenchymal cells from each tissue section was carried out using Histodenz.

Subcutaneous tumor implantation in immunosuppressed and immunocompetent mice. For assessment of the in vivo tumor growth, 6 to eight-week-old male athymic N:NIH(S)-nu mice (Nu/Nu), and C3H/He mice (n = 4/group) were subcutaneously (s.c.) injected into the right flank with 1×10^5 CD133 + Hepa129 cells, 1×10^5 4Mu-treated CD133 + Hepa129 cells, 1×10^5 CD133-Hepa129 cells and 1×10^5 4Mu-treated CD133- Hepa129 cells. Tumor volume was determined as above. Also, Nu/Nu and C3H/He mice (n = 4) were s.c. injected with Hepa129 + conditioned medium from peritoneal macrophages (pMϕ derived-CM) and Hepa129 + 4Mu-treated pMϕ derived-CM (described below).

Mice vaccination with DCs. HCC tumors were induced s.c. in C3H/He mice (n = 4–5/group) by inoculating 1×10^6 Hepa129 cells, or in BALB/c mice (n = 4/group) by inoculating BNL cells. Tumors were detected approximately 10 days after injection. Then, 1×10^5 matured DCs, or DCs loaded with lysates were injected peritumorally into tumor-bearing mice. Tumor growth was measured 3 times per week, and volumes were calculated as described above.

Ex vivo experiments.
Macrophages profile assessment. Histodenz isolated liver cells were cultured for 30 min. Then, cells adhered to plastic were collected, and used for flow cytometry analysis or stored at −80 °C with Trizol (Invitrogen, USA) for further RNA isolation. Flow cytometry of F4/80+, CD206+ and CD86+ were performed using a FACS Aria (BD Biosciences, USA). For FACS, potential autofluorescence of 4Mu was ex-

	Forward	Reverse	Primer efficacy (%)	PCR efficiency (%)
TNF-α	5′-GACCCTCACACTCAGATCATC TTCT-3′	5′-CCACTTGGTGTTTTGCTA CGA-3′	125.42	94.40
iNOS	5′-AAGATGGCCTGGAGGAATGC-3′	5′-TGCTGTGCTACAGTTCCGAG-3′	113.59	94.59
Arg1	5′-CAGAAGATTGGAAGAGTCAG-3′	5′-CAGATATGCAGGGAGTCACC-3′	105.68	94.80
IL-10	5′-GGTTGCCAAGCCTTATCGGA-3′	5′-ACCTGCTCCACTGCCTTGCT-3′	101.74	94.46
IL-1b	5′-TGACAGTGATGAGAATGACCT GTTC-3′	5′-TTGGAAGCAGCCCTTCATCT-3′	116.62	94.70
GAPDH	5′-CATCTCTGCCCCCTCTGCTG-3′	5′-GCCTGCTTCACCACCTTC TTG-3′	136.12	95.50

Table 1. Specific forward and reverse primers.

cluded in all studies and fluorescence minus one controls (FMO) were performed using BD CompBead particles (Cat No 560499). For accurately, gates were placed at the FMO staining. Macrophages type1/type2 proportion was calculated as log10 (CD86+/CD206+).

RNA isolation and quantitative PCR analysis. total RNA samples were isolated using Trizol Reagent (Sigma-Aldrich Co) and Total RNA (2 mg) was reverse transcribed (RT-qPCR) with 200 U of SuperScript II Reverse Transcriptase (Invitrogen) using 500 ng of Oligo (dT) primers. cDNAs were subjected to real time polymerase chain reaction (qPCR) (Stratagene Mx3005p, Stratagene, La Jolla, CA, USA) as we previously described[25]. The mRNA levels of inducible Nitric Oxide Sintetase (iNOS), interleukin-1b (IL-1β), Tumor Necrosis Factor alpha (TNF-α), Arginase I, interleukin-10 (IL-10) and Transforming Growth Factor beta (TGF-β) were quantified using SYBRGreen (Invitrogen); amplifications were carried out using a cycle of 95 °C for 10 min and 40 cycles under the following parameters: 95 °C for 30 s, 56 °C for 30 s, 72 °C for 1 min. At the end of PCR reaction, temperature was increased from 60 to 95 °C at a rate of 2 °C/min, and fluorescence was measured every 15 s to construct the melting curve. Values were normalized to levels of glyceraldehyde-3-phosphate dehydrogenase transcript GAPDH used as housekeeping. The expression of GAPDH was not significantly different between groups. Data were processed by the ΔΔCt method. The relative amount of the PCR product amplified from untreated macrophages or saline (control) tumor tissue samples were set as 1. A non-template control (NTC) was run in every assay, and all determinations were performed as triplicates for each animal in two separated experiments. The relative expression was calculated according to the equation Rel. Exp (RE) = $2^{-\Delta\Delta Ct}$. List of primers are detailed in the Table 1. The primer efficacy (PE) was calculated according to the equation PE (%) = $\{[10^{(-1/m)}] - 1\} \times 100$, m = slope and the PCR efficiency was shown by the LinRegPCR program[47] Version 11.0.

Isolation of intraperitoneal macrophages. Macrophages were isolated from the peritoneal cavity (pMφ), incubated in serum-free medium for 30 min in a 24-well tissue-culture plate, and treated with 0.5 mM 4Mu or RPMI for additional 72 h. Then, cells were collected and used for flow cytometry analysis or maintained with Trizol (Invitrogen, USA) at − 80 °C. In addition, conditioned medium (CM) from 4Mu-treated pMφ (4Mu-treated pMφ derived-CM) or pMφ derived-CM was stored at − 80 °C until its use. Flow cytometry of F4/80+, CD206+ and CD86+ were performed using a FACSAria (BD Biosciences, USA), macrophages type1/type2 proportion was calculated as above and quantitative PCR analysis were performed as we described above.

Hepa129 cells were incubated with RPMI (Hepa129 + RPMI), CM from isolated pMφ (Hepa129 + pMφ derived-CM) and conditioned media from isolated pMφ in vitro treated with 4Mu (Hepa129 + 4Mu treated-pMφ derived-CM) for 48 h. Preconditioned 1 × 10⁶ Hepa129 cells were used for in vivo experiments or for western blot. Intraperitoneal Mφ also were obtained on day 9 and day 15 from mice with fibrosis-associated HCC treated with saline or 20 mg/kg 4Mu. Flow cytometry of F4/80 + CD86+ and CD206+ cells also were analyzed and the M1/M2 proportions were calculated as above.

Quantification of CD3+ cells on HCC tumors. Tumor lysates from mice treated with 4Mu or saline were obtained after liver perfusion with collagenase (Sigma-Aldrich, USA). Cell suspensions were then treated with RBC lysis buffer and stained with anti-CD4, anti-CD8, and anti-CD3 antibodies (BD Biosciences, USA). Then, lymphocytic infiltrate on tumor tissue was analyzed by flow cytometry.

Quantification of splenic CD11b+Gr1+ and CD4+ Foxp3+ cells from HCC-bearing mice. single cell suspensions of splenocytes were prepared, and resuspended in PBS (phosphate buffer solution). Cell suspensions were treated with red blood cell lysis buffer (0.15 M NH4Cl, 1 mM KHCO3, 0.1 mM Na2–EDTA), and washed with PBS 1% BSA. Splenocytes were stained with different conjugated-antibodies: anti Foxp3-PE (eBiosciences, USA), anti CD4-FITC, anti CD11b-APC, and anti-Gr1-PE (BD Biosciences, USA) and their respective isotypes. Then, cells were fixed with 1% paraformaldehyde and subjected to flow cytometry (Accuri 6C, BD, USA). Data were analyzed using Accuri 6C software.

Westen blotting. expression of TLR4, Sox2 and CD47 was detected in extracts from preconditioned whole, CD133+ or CD133- Hepa129 cells by immunoblotting. Briefly, cells were collected and incubated in lysis buffer

with protease inhibitors (50 mM Tris-HCl buffer, pH7.4, containing 0.1% Tween-20, 150 mM NaCl, 10 μg/ml aprotinin, 5 μg/ml leupeptin, 1 mM PMSF) 30 min on ice. Measurement of total protein concentration was performed using Bradford assay. Then, 50 μg of total protein was loaded and separated on 10% SDS-PAGE gels and transferred to polyvinylidene difluoride[48]. Blots were then developed with 1:500 mouse anti-TLR4 (Santa Cruz Biotechnology)[49]; 1:2000 rabbit anti-SOX2 (Santa Cruz Biotechnology)[50] 1:1000 rat anti-CD47 (Abcam)[51] and 1:5000 horseradish peroxidase (HRP)-conjugated goat anti-mouse antibody (Jackson ImmunoResearch Labs,USA)[52]. Bands were detected using the ECL detection system. Protein loading and transfer was monitored using an anti-actin antibody (1:1000, Santa Cruz Biotechnology, USA)[53] and incubated with HRP-goat anti-mouse antibody (diluted 1/5000, Santa Cruz Biotechnology, USA)[52]. Bands intensities were measured by densitometer analysis using the Scion Image software (Scion Corporation, USA).

IL-6 quantification.   To characterize conditioned medium, supernatants of pMϕ were collected 72 h after being treated with 4Mu, replaced with RPMI serum-free and collected after 24 and 48 h of culture. The concentration of IL-6 was measured by ELISA from BD (BD Biosciences, USA) according to the manufacture's guideline.

Generation of bone marrow-derived DCs.   DCs were generated from murine bone marrow cells as described previously[54]. Briefly, bone marrow of C3H/He mice or BALB/c were obtained from femurs and tibias, subjected to mechanic disruption, cell suspensions obtained and cultured with RPMI 1640 with 10% FBS, and IL-4 and GM-CSF (20 ng/ml; PeproTech, Germany). On day 3 and 5, the medium was withdrawn and replaced by new fresh RPMI. On day 7, suspension cells were collected (DCs) and used for experiments.

Phenotypic analysis of DCs.   DCs were cultured with 0.5 mM 4Mu during 72 h. Then, DCs were stained with CD11c-PE, CD86-APC, and MCH-II-FITC (BD Biosciences, USA) and analyzed by flow cytometry.

Phagocytosis assay.   DCs (5×10^4) were immunostained with anti-CD11c, CD86 and MHCII and exposed to whole, CD133 + , CD133- Hepa129 cells treated or not with 4Mu (5×10^5), labeled with DAPI and incubated for 2 h at 37 °C. Phagocytosis was determined by flow cytometry detection of CD11+ CD86+ MHCII+ DAPI+ cells.

Antigen loading.   Hepa129, BNL cells or tumor extracts from HCC bearing-mice were obtain as previously[54]. Briefly, DCs were pulsed with cells or tumor lysates alone (200 μg/10⁶ cells/ml) at 37 °C for 18 h. Cells were then centrifuged, characterized by flow cytometry, and used for in vivo experiments.

In vitro assays.   *Cell isolation by magnetic-activated cell sorting (MACS).*   Hepa129 cells were labeled with primary CD133/1 antibody (Miltenyi Biotec, Germany), and the CD133 + was subsequently magnetically isolated using MACS Columns.

Statistical analysis.   All experiments were repeated at least 2 or 3 times on different occasions. Values were expressed as the mean ± SEM. Mann–Whitney, Tukey's or Kruskall–Wallis (ANOVA) multiple comparison tests were used to evaluate the statistical differences between groups. Mice survival was analyzed by a Kaplan–Meier curve. P value < 0.05 was considered as significant. Prism software (Graph Pad, San Diego, CA, USA) was employed for the statistical analysis[25].

References

1. Bray, F. *et al.* Global cancer statistics 2018: GLOBOCAN estimates of incidence and mortality worldwide for 36 cancers in 185 countries. *CA Cancer J. Clin.* **68**, 394–424. https://doi.org/10.3322/caac.21492 (2018).
2. Forner, A., Reig, M. & Bruix, J. Hepatocellular carcinoma. *Lancet* **391**, 1301–1314. https://doi.org/10.1016/S0140-6736(18)30010-2 (2018).
3. Llovet, J. M. *et al.* Sorafenib in advanced hepatocellular carcinoma. *N. Engl. J. Med.* **359**, 378–390. https://doi.org/10.1056/NEJMoa0708857 (2008).
4. Bruix, J. *et al.* Regorafenib for patients with hepatocellular carcinoma who progressed on sorafenib treatment (RESORCE): A randomised, double-blind, placebo-controlled, phase 3 trial. *Lancet* **389**, 56–66. https://doi.org/10.1016/S0140-6736(16)32453-9 (2017).
5. Llovet, J. M., Montal, R., Sia, D. & Finn, R. S. Molecular therapies and precision medicine for hepatocellular carcinoma. *Nat. Rev. Clin. Oncol.* **15**, 599–616. https://doi.org/10.1038/s41571-018-0073-4 (2018).
6. Vrecko, S. *et al.* Personalized identification of tumor-associated immunogenic neoepitopes in hepatocellular carcinoma in complete remission after sorafenib treatment. *Oncotarget* **9**, 35394–35407. https://doi.org/10.18632/oncotarget.26247 (2018).
7. Pardee, A. D. & Butterfield, L. H. Immunotherapy of hepatocellular carcinoma: Unique challenges and clinical opportunities. *Oncoimmunology* **1**, 48–55. https://doi.org/10.4161/onci.1.1.18344 (2012).
8. Breous, E. & Thimme, R. Potential of immunotherapy for hepatocellular carcinoma. *J. Hepatol.* **54**, 830–834. https://doi.org/10.1016/j.jhep.2010.10.013 (2011).
9. El-Khoueiry, A. B. *et al.* Nivolumab in patients with advanced hepatocellular carcinoma (CheckMate 040): An open-label, non-comparative, phase 1/2 dose escalation and expansion trial. *Lancet* **389**, 2492–2502. https://doi.org/10.1016/S0140-6736(17)31046-2 (2017).
10. Duffy, A. G. *et al.* Tremelimumab in combination with ablation in patients with advanced hepatocellular carcinoma. *J. Hepatol.* **66**, 545–551. https://doi.org/10.1016/j.jhep.2016.10.029 (2017).

11. Administration, U. S. F. A. D. *FDA Grants Accelerated Approval to Nivolumab and Ipilimumab Combination for Hepatocellular Carcinoma* (2020). https://www.fda.gov/drugs/resources-information-approved-drugs/fda-grants-accelerated-approval-nivolumab-and-ipilimumab-combination-hepatocellular-carcinoma. Accesed 21 April 2020

12. Yarchoan, M. *et al.* Characterization of the immune microenvironment in hepatocellular carcinoma. *Clin. Cancer Res.* **23**, 7333–7339. https://doi.org/10.1158/1078-0432.CCR-17-0950 (2017).

13. Roth, G. S. & Decaens, T. Liver immunotolerance and hepatocellular carcinoma: Patho-physiological mechanisms and therapeutic perspectives. *Eur. J. Cancer* **87**, 101–112. https://doi.org/10.1016/j.ejca.2017.10.010 (2017).

14. Hernandez-Gea, V., Toffanin, S., Friedman, S. L. & Llovet, J. M. Role of the microenvironment in the pathogenesis and treatment of hepatocellular carcinoma. *Gastroenterology* **144**, 512–527. https://doi.org/10.1053/j.gastro.2013.01.002 (2013).

15. Yeung, O. W. *et al.* Alternatively activated (M2) macrophages promote tumour growth and invasiveness in hepatocellular carcinoma. *J. Hepatol.* **62**, 607–616. https://doi.org/10.1016/j.jhep.2014.10.029 (2015).

16. Mantovani, A., Germano, G., Marchesi, F., Locatelli, M. & Biswas, S. K. Cancer-promoting tumor-associated macrophages: New vistas and open questions. *Eur. J. Immunol.* **41**, 2522–2525. https://doi.org/10.1002/eji.201141894 (2011).

17. Yunna, C., Mengru, H., Lei, W. & Weidong, C. Macrophage M1/M2 polarization. *Eur. J. Pharmacol.* **877**, 173090. https://doi.org/10.1016/j.ejphar.2020.173090 (2020).

18. Dong, N. *et al.* M2 macrophages mediate sorafenib resistance by secreting HGF in a feed-forward manner in hepatocellular carcinoma. *Br. J. Cancer* **121**, 22–33. https://doi.org/10.1038/s41416-019-0482-x (2019).

19. Wu, Q. *et al.* Blocking triggering receptor expressed on myeloid cells-1-POSITIVE TUMor-associated macrophages induced by hypoxia reverses immunosuppression and anti-programmed cell death ligand 1 resistance in liver cancer. *Hepatology* **70**, 198–214. https://doi.org/10.1002/hep.30593 (2019).

20. Reya, T., Morrison, S. J., Clarke, M. F. & Weissman, I. L. Stem cells, cancer, and cancer stem cells. *Nature* **414**, 105–111. https://doi.org/10.1038/35102167 (2001).

21. Yang, Z. F. *et al.* Identification of local and circulating cancer stem cells in human liver cancer. *Hepatology* **47**, 919–928. https://doi.org/10.1002/hep.22082 (2008).

22. Bao, B., Ahmad, A., Azmi, A. S., Ali, S. & Sarkar, F. H. Overview of cancer stem cells (CSCs) and mechanisms of their regulation: Implications for cancer therapy. *Curr. Protoc. Pharmacol.* https://doi.org/10.1002/0471141755.ph1425s61 (2013).

23. Jun, S. Y. *et al.* The positive correlation of TIPRL with LC3 and CD133 contributes to cancer aggressiveness: Potential biomarkers for early liver cancer. *Sci. Rep.* **9**, 16802. https://doi.org/10.1038/s41598-019-53191-5 (2019).

24. Wan, S. *et al.* Tumor-associated macrophages produce interleukin 6 and signal via STAT3 to promote expansion of human hepatocellular carcinoma stem cells. *Gastroenterology* **147**, 1393–1404. https://doi.org/10.1053/j.gastro.2014.08.039 (2014).

25. Rodriguez, M. M. *et al.* 4Mu decreases CD47 expression on hepatic cancer stem cells and primes a potent antitumor T cell response induced by interleukin-12. *Mol. Ther.* **26**, 2738–2750. https://doi.org/10.1016/j.ymthe.2018.09.012 (2018).

26. Krenkel, O. & Tacke, F. Liver macrophages in tissue homeostasis and disease. *Nat. Rev. Immunol.* **17**, 306–321. https://doi.org/10.1038/nri.2017.11 (2017).

27. Piccioni, F. *et al.* Antitumor effects of hyaluronic acid inhibitor 4-methylumbelliferone in an orthotopic hepatocellular carcinoma model in mice. *Glycobiology* **22**, 400–410. https://doi.org/10.1093/glycob/cwr158 (2012).

28. Piccioni, F. *et al.* 4-methylumbelliferone inhibits hepatocellular carcinoma growth by decreasing IL-6 production and angiogenesis. *Glycobiology* **25**, 825–835. https://doi.org/10.1093/glycob/cwv023 (2015).

29. Hussain, S. & Stohlman, S. A. Peritoneal macrophage from male and female SJL mice differ in IL-10 expression and macrophage maturation. *J. Leukoc. Biol.* **91**, 571–579. https://doi.org/10.1189/jlb.0711351 (2012).

30. Liu, W. T. *et al.* Toll like receptor 4 facilitates invasion and migration as a cancer stem cell marker in hepatocellular carcinoma. *Cancer Lett.* **358**, 136–143. https://doi.org/10.1016/j.canlet.2014.12.019 (2015).

31. Lee, T. K. *et al.* Blockade of CD47-mediated cathepsin S/protease-activated receptor 2 signaling provides a therapeutic target for hepatocellular carcinoma. *Hepatology* **60**, 179–191. https://doi.org/10.1002/hep.27070 (2014).

32. Liu, L. *et al.* SIRT1-mediated transcriptional regulation of SOX2 is important for self-renewal of liver cancer stem cells. *Hepatology* **64**, 814–827. https://doi.org/10.1002/hep.28690 (2016).

33. Mishra, L. *et al.* Liver stem cells and hepatocellular carcinoma. *Hepatology* **49**, 318–329. https://doi.org/10.1002/hep.22704 (2009).

34. Hanahan, D. & Coussens, L. M. Accessories to the crime: functions of cells recruited to the tumor microenvironment. *Cancer Cell* **21**, 309–322. https://doi.org/10.1016/j.ccr.2012.02.022 (2012).

35. Karlmark, K. R. *et al.* Hepatic recruitment of the inflammatory Gr1+ monocyte subset upon liver injury promotes hepatic fibrosis. *Hepatology* **50**, 261–274. https://doi.org/10.1002/hep.22950 (2009).

36. Sun, Y. F. *et al.* Circulating stem cell-like epithelial cell adhesion molecule-positive tumor cells indicate poor prognosis of hepatocellular carcinoma after curative resection. *Hepatology* **57**, 1458–1468. https://doi.org/10.1002/hep.26151 (2013).

37. Fan, Q. M. *et al.* Tumor-associated macrophages promote cancer stem cell-like properties via transforming growth factor-beta1-induced epithelial-mesenchymal transition in hepatocellular carcinoma. *Cancer Lett.* **352**, 160–168. https://doi.org/10.1016/j.canlet.2014.05.008 (2014).

38. Blois, S. M. *et al.* Dendritic cells regulate angiogenesis associated with liver fibrogenesis. *Angiogenesis* **17**, 119–128. https://doi.org/10.1007/s10456-013-9382-5 (2014).

39. Chen, J. *et al.* Macrophages induce CD47 upregulation via IL-6 and correlate with poor survival in hepatocellular carcinoma patients. *Oncoimmunology* **8**, e1652540. https://doi.org/10.1080/2162402X.2019.1652540 (2019).

40. Sangro, B. *et al.* Diagnosis and management of toxicities of immune checkpoint inhibitors in hepatocellular carcinoma. *J. Hepatol.* **72**, 320–341. https://doi.org/10.1016/j.jhep.2019.10.021 (2020).

41. Tovar, V. *et al.* Tumour initiating cells and IGF/FGF signalling contribute to sorafenib resistance in hepatocellular carcinoma. *Gut* **66**, 530–540. https://doi.org/10.1136/gutjnl-2015-309501 (2017).

42. Lo, J. *et al.* Nuclear factor kappa B-mediated CD47 up-regulation promotes sorafenib resistance and its blockade synergizes the effect of sorafenib in hepatocellular carcinoma in mice. *Hepatology* **62**, 534–545. https://doi.org/10.1002/hep.27859 (2015).

43. Binnewies, M. *et al.* Unleashing type-2 dendritic cells to drive protective antitumor CD4(+) T cell immunity. *Cell* **177**, 556–571. https://doi.org/10.1016/j.cell.2019.02.005 (2019).

44. Salmon, H. *et al.* Expansion and activation of CD103(+) dendritic cell progenitors at the tumor site enhances tumor responses to therapeutic PD-L1 and BRAF inhibition. *Immunity* **44**, 924–938. https://doi.org/10.1016/j.immuni.2016.03.012 (2016).

45. Palmer, D. H. *et al.* A phase II study of adoptive immunotherapy using dendritic cells pulsed with tumor lysate in patients with hepatocellular carcinoma. *Hepatology* **49**, 124–132. https://doi.org/10.1002/hep.22626 (2009).

46. Cao, J., Kong, F. H., Liu, X. & Wang, X. B. Immunotherapy with dendritic cells and cytokine-induced killer cells for hepatocellular carcinoma: A meta-analysis. *World J. Gastroenterol.* **25**, 3649–3663. https://doi.org/10.3748/wjg.v25.i27.3649 (2019).

47. Ruijter, J. M. *et al.* Amplification efficiency: Linking baseline and bias in the analysis of quantitative PCR data. *Nucleic Acids Res* **37**, e45. https://doi.org/10.1093/nar/gkp045 (2009).

48. Atorrasagasti, C. *et al.* Overexpression of SPARC obliterates the in vivo tumorigenicity of human hepatocellular carcinoma cells. *Int. J. Cancer* **126**, 2726–2740. https://doi.org/10.1002/ijc.24966 (2010).

49. Park, H. S. *et al.* Mycobacterium tuberculosis Rv3463 induces mycobactericidal activity in macrophages by enhancing phagolysosomal fusion and exhibits therapeutic potential. *Sci. Rep.* **9**, 4246. https://doi.org/10.1038/s41598-019-38982-0 (2019).

50. Cui, C. P. *et al.* Dynamic ubiquitylation of Sox2 regulates proteostasis and governs neural progenitor cell differentiation. *Nat. Commun.* **9**, 4648. https://doi.org/10.1038/s41467-018-07025-z (2018).
51. Wu, L. *et al.* Anti-CD47 treatment enhances anti-tumor T-cell immunity and improves immunosuppressive environment in head and neck squamous cell carcinoma. *Oncoimmunology* **7**, e1397248. https://doi.org/10.1080/2162402X.2017.1397248 (2018).
52. Song, L. *et al.* Proto-oncogene Src links lipogenesis via lipin-1 to breast cancer malignancy. *Nat. Commun.* **11**, 5842. https://doi.org/10.1038/s41467-020-19694-w (2020).
53. Hwang, H. & Rhim, H. Acutely elevated O-GlcNAcylation suppresses hippocampal activity by modulating both intrinsic and synaptic excitability factors. *Sci. Rep.* **9**, 7287. https://doi.org/10.1038/s41598-019-43017-9 (2019).
54. Rizzo, M. *et al.* Low molecular weight hyaluronan-pulsed human dendritic cells showed increased migration capacity and induced resistance to tumor chemoattraction. *PLoS ONE* **9**, e107944. https://doi.org/10.1371/journal.pone.0107944 (2014).

Acknowledgements

Author contributions

Conception and design: M.M. and G.M.; Development of methodology: M.M.R. and M.M.; Acquisition of data: M.M.R., E.F. and A.O.; Analysis and interpretation of data: M.M.R., M.M. and G.M.; Writing, review, and/or revision of the manuscript: M.M., J.B., M.G., A.C. and G.M.; Administrative, technical, or material support: M.J.C., C.A., M.G., A.O. and L.D.; Study supervision: G.M.

Competing interests

The authors declare no competing interests.

Additional information

Supplementary Information The online version contains supplementary material available at https://doi.org/10.1038/s41598-021-85491-0.

Correspondence and requests for materials should be addressed to G.D.M.

Reprints and permissions information is available at www.nature.com/reprints.

Publisher's note Springer Nature remains neutral with regard to jurisdictional claims in published maps and institutional affiliations.